Arch. Metall. Mater. **64** (2019), 4, 1207-1212

DOI: 10.24425/amm.2019.130082

M. JASIŃSKI*#, K. ZIEWIEC*, M. WOJCIECHOWSKA*

REAL TIME THERMAL IMAGING OF SOLID OXIDE FUEL CELL

In this work, a mid infrared thermography was used to study thermal behavior of solid oxide fuel cell (SOFC) with a circular shape and a diameter of 90 mm. The emissivity of the anodic surface of the fuel cell was determined to be from 0.95 to 0.46 in the temperature range 550-1200 K and the profile and temperature distribution of the anodic surface of the unloaded cell was given. The surface temperature of the cell was determined during operation and the polarity changes from open circuit voltage (OCV) to 0.0 V. It was found that the cell self-heating effect decreases with increasing temperature of the cell.

Keywords: thermography, solid oxide fuel cell, sofc, thermal imaging, infrared

1. Introduction

The development of human civilization is inevitably accompanied by an increasing need for useful forms of energy, such as electricity, mechanical energy and heat. An effective solution to cover this need is the implementation of methods that are much more efficient than traditional getting electricity from available fossil fuels. Such methods mainly involve the production of electricity using fuel cells. Solid oxide fuel cells (SOFCs) are promising devices for the production of electricity and heat in combined systems (CHP – cogenerate heat and power) [1,2]. Fuel cells have many advantages over conventional methods of generating electricity such as much higher electrical efficiency, very low gas emissions and voiceless.

One of the most serious problems with the use of SOFCs is the use of materials for their construction, providing their chemical, structural, electrical and thermo-mechanical properties for a long time under conditions of high temperature and pressure. A comprehensive approach to these problems is possible using electrochemical research methods such as impedance spectroscopy or voltammetry [3,4]. However, these methods are not able to identify local chemical processes in situ at the cell. For proper control of the cell, it is possible to place a temperature measuring device (thermocouple) close to it. This allows mapping the temperature of a single cell or a set of such cells (fuel cell stack) [5]. Placing the thermocouple as close to the cell's surface as possible may lead to its penetration, deterioration and finally to its destruction. Adzic [6] used a flat thermocouple for measuring temperature in SOFC cells and placed it at a distance of about 5 μm above the surface of the cell. However, the measured temperatures differed significantly from the surface temperature of the electrode. Mid-infrared thermography is a method that allows observation of the electrode surface of the cell and its temperature characteristics providing much more detailed information about the processes running on the surface of the working cell in comparison with the use of point temperature measurement using a thermocouple. This method was used in PEM (polymer electrolyte membrane) cells to measure current density, the influence of fuel saturation with steam or fuel type [7,8]. Research on SOFC cells confirms the potential of the thermography for testing small (several millimetres in diameter) cells [9,10]. Thermal imaging of cells working in hydrogen, ethanol, propane, and biogas was carried out [9-12], as well as correlated with other methods such as synchrotron x-ray diffraction [13] and Fourier-transform infrared emission spectra [14]. Previous research has been done on small (up to 25 mm in diameter) button or pellet cells [9,10]. Also, recent studies of SOFC cells confirm the potential of the thermography method for testing small (several millimetres in diameter) cells [9,10]. At the same time, Brett [11] together with co-authors indicates the need to investigate larger SOFC fuel cells than before, due to the low resolution of temperature changes during the operation of the low-dimension fuel cells. The aim of this work is to study the thermal phenomena on the surface of the fuel cells with better space and temperature resolution than it was done in the previous research.

2. Experimental

The SOFC used in the experiment was a commercially available cell with a diameter of 90 mm from Cerel (PL). The cell with a thickness of about 1050 μm is anode supported cell

* INSTITUTE OF TECHNOLOGY, PEDAGOGICAL UNIVERSITY, 2 PODCHORĄŻYCH STR., 30-084 KRAKÓW, POLAND

Corresponding author: marcin.jasinski@up.krakow.pl

and the composition: NiO/8YSZ anode (TOSOH), electrolyte 8YSZ (TOSOH) and cathode $La_{0.6}Sr_{0.4}Fe_{0.8}Co_{0.2}O_{3-\delta}$ (Praxair). The cell was made using the high-pressure injection-moulding and screen printing methods described elsewhere [15]. The measuring holder together with the mounted cell was placed in a tubular furnace – arranged horizontally with an inner diameter of 150 mm. The experimental setup together with the measuring holder was designed according to the project of the set-up described in [9], after making appropriate changes. Metal electrodes – current collectors: a platinum grid on the cathode side and a nickel grid on the anode side – have been applied to the surface of the cell. The tested cell was placed along inside the furnace with the applied electrodes, electrical connections and thermocouple. Fuel and air were continuously supplied to the cell. In order to minimize the influence of stresses on the fuel cell and work pipe, a gradient connection system with different coefficient of thermal expansion was used. An important element of the installation was a steel pipe placed between the cell and the working pipe. The emissivity of the anodic surface of the cell was determined on the basis of K-type thermocouple measurements and thermovisual observations at different temperatures after obtaining a steady state were made. The SOFC's anode side was facing towards the FLIR (MID-IR InSb) lens camera. The camera is equipped with a 25 mK high-sensitivity InSb detector cooled to 85 K. Images were recorded at a maximum resolution of 640x512 pixels at 100 Hz. Thermography observations were conducted through a quartz window.

The emissivity measurement was carried out in the temperature range of 550-1200 K. After determining the dependence of the emissivity on the temperature, the working cell was observed using infrared radiation. All flows were regulated with mass flow controllers (Brooks 4850) and constant flows of 1000 sccm 4% of H_2 in Ar by volume and 1000 sccm synthetic air were delivered to the anode and the cathode, respectively. Cell polarization was maintained and electrochemical measurements were conducted with a potentiostat build in-house. The current-voltage characteristics of the fuel cell were determined.

3. Results and discussion

The graph of the determined cell emissivity as a function of temperature is presented in Fig. 1. The results obtained in the present work indicate that the emissivity decreases with the increase of temperature. Initially, in the range from 550 to 735 K, the emissivity is at 0.95. As the temperature rises further, the emissivity decreases continuously. In the temperature range relevant for the cell operation from 880 K to 1200 K, the emissivity of the anode surface of the cell varies from 0.66 to 0.46, respectively. The above characteristics of emission changes are similar to the results presented in P.E. Liley [16] for ZrO_2. A large number of cavities and the porous surface of the anode may be the reason for its high emissivity. It is worth to mention, that tested cell material in addition to ZrO_2 also contains up to 50% NiO, and after the reduction also Ni, which may affect a slightly different thermal emissivity characteristic [17,18]. In works [9,10,13,14] using an infrared camera, the emissivity of the cell's surface was not given. Due to the significant influence of emissivity on the observed apparent temperature values during thermal imaging studies in the present work, this important thermography parameter was estimated.

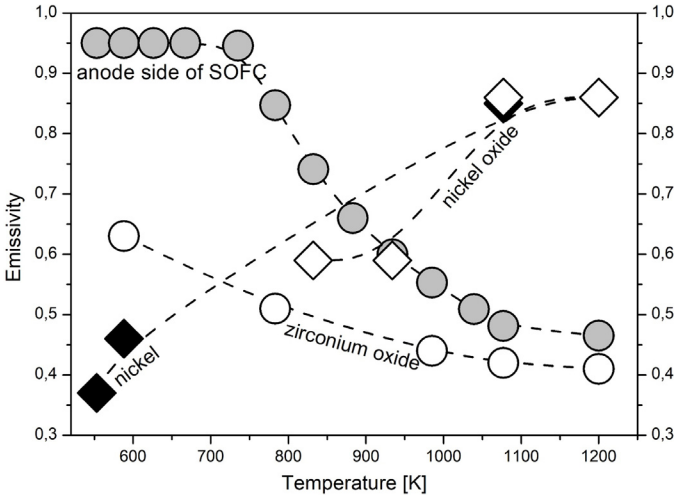

Fig. 1. Emissivity curves: (grey circles: SOFC's anode side, white circles: ZrO_2, black squares: Ni, white squares: NiO) [16-18]

In another work, Pomfret [9] adjusted the temperature from the thermal imaging camera to the temperature of the thermocouple using a coefficient which he called Intensity. The emissivity determination method used in this work seems to be a much more reliable method than that proposed by other authors [12], because it allows for more accurate emissivity determination at different temperatures, in stable temperature conditions, and eliminates the influence of the outside atmosphere on the measurement.

Emissivity values equal to one that other authors received [11,12] should be treated as a simplifying assumption because such emissivity has a perfectly black body. Therefore, the method used in this work complements the existing data.

Fig. 2c shows the results of thermography measurements at 1200 K, for which the emissivity was 0.46. Profiles were applied along the lines shown in Fig. 2a (ROI1 and ROI2). The results presented in Fig. 2c shows that the temperature distribution in both the x and y-axes is uneven. For a horizontal temperature distribution, the temperature profile is symmetrical and the difference between the centre and the outermost surfaces of the cell varies depending on the temperature and ranges from 12 to 19 K in the temperature range from 800 K to 1200 K. The vertical temperature profile is asymmetrical. Cell surfaces located above have higher temperatures than those located below. The temperature difference between the centre and the outermost surfaces of the cell varies depending on the temperature and ranges from 14 to 29 K.

At the walls of the furnace, the surface temperature of the cell is higher than in the central areas, due to the closer presence of heating elements. Differences in the cell surface temperature along the horizontal profile were also determined by other

authors [10,11,19] and have a similar character, however, due to the larger size of the cell shown in this paper (90 mm), the differences in the gradient are 2-3 times greater than presented in the aforementioned works [10,11,19].

There is no information in the literature about cell surface distribution along with the vertical profile. Assuming a constant temperature of the internal surfaces of the furnace, large differences in the temperature between the cell surfaces located higher and lower can be caused by several factors: the large diameter of the furnace pipe (150 mm), conduction, radiation and convection of heat, and gas flow. The pipe with the cell is supported on ceramic support, hence the process of heat transfer up the cell should be taken into account [20]. Also, the heat convection process in the cell chamber can be responsible for the asymmetry of the temperature distribution along with the vertical profile [20]. Finally, any object with a temperature higher than absolute zero radiates energy, according to the emissivity value of its surface [21]. The outflow of combustible gas and air occurred at the bottom of the cell, which is why the lower parts of the cell may have a lower temperature [22].

The results of maximum and minimum temperature measurements along horizontal and vertical profiles in the 1200 K are shown in Fig. 2d also indicates the results of temperature measurements from the field marked in Fig. 2b as ROI3.

The temperature from the ROI3 profile is located between the lines representing the maximum and minimum temperatures from the ROI1 and ROI2 profiles and can be treated as the average surface temperature of the cell for further cell measurements during operation.

Temperature differences in the plane of the cell shown in Fig. 2 can affect its mechanical stability and the formation of stresses inside the cell. The linear thermal expansion coefficients α (CTE) of materials for SOFC construction at temperatures between 550 and 1200 K range from 10.5 to 12.5 $10^{-6}\,K^{-1}$ [23,24].

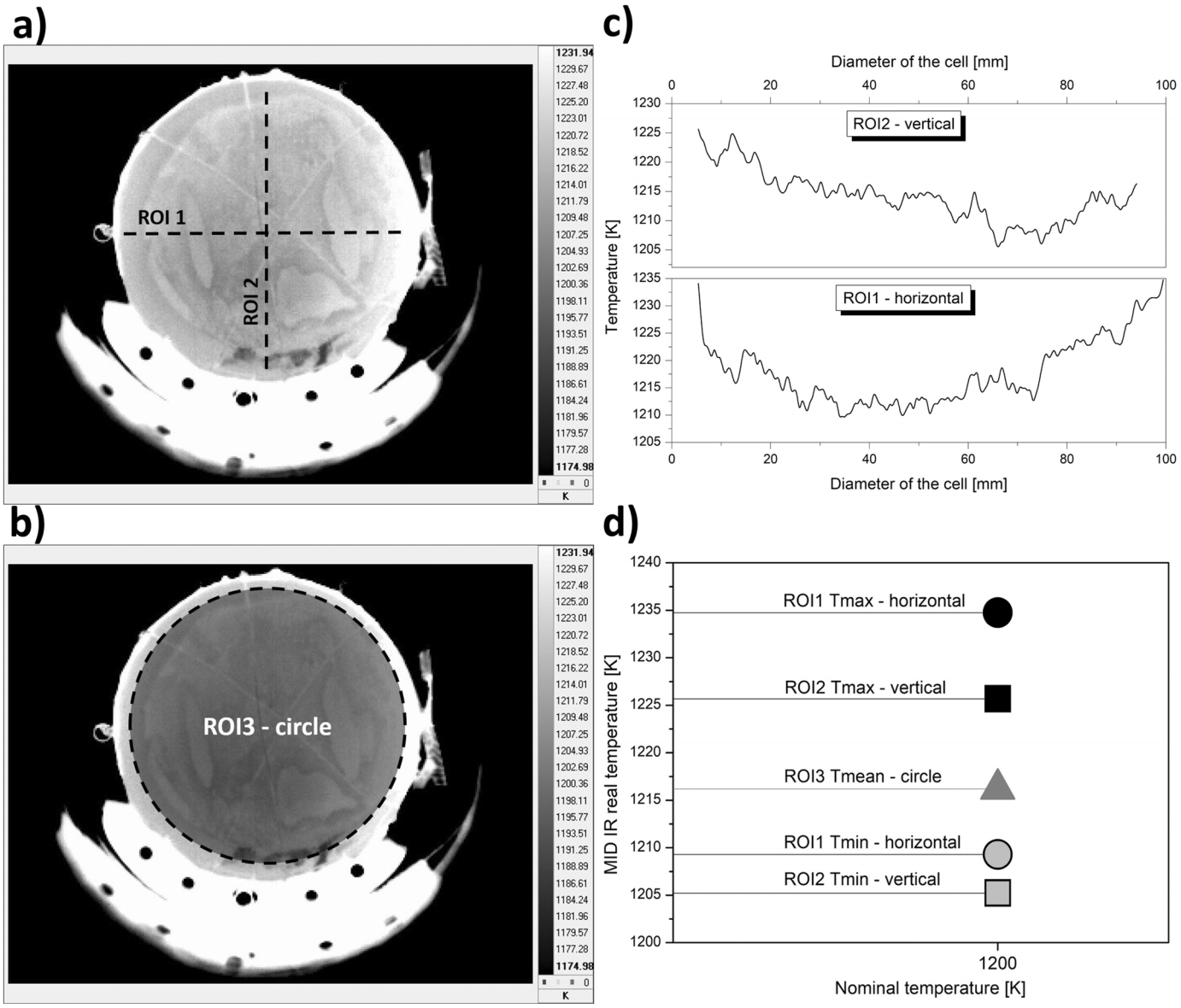

Fig. 2. Thermal images at 1200 K – a) and b); intermediate lines ROI1 and ROI2 are marked horizontal and vertical profiles. ROI3 shows the circular distribution of temperature. Temperature charts at 1200 K – c) and d); temperature graphs for ROI1 and ROI2 profiles. Chart of the minimum and maximum temperatures read from the ROI1 and ROI2 profiles for individual measurements and temperature from the ROI3 field – d)

The higher the temperature differences, the more they affect the amount of tensile and compressive stresses that arise in the material, which can lead to cracks and destruction of the material. In other works [9-14,19,25,26], due to the smaller size of cells, the question of stressing due to the influence of temperature was not discussed, but it was possible in our work, thanks to the possibility of testing full-size fuel cells.

The relationships between the electrical load of the cell and the temperature of its surface were investigated by changing the voltage and observing changes in the current and surface temperature of the cell. After determining the voltage and current density, surface temperature polarization curves of the SOFC fuel cell in the temperature range 900-1200 K in 4% H_2/Ar flow were plotted. As the temperature increases, OCV and the cell's power increases. At 900, 1000, 1100 and 1200 K, OCV was 0.97, 0.98, 0,99 and 1.01 V, while the maximum cell power was 0.51; 1.58; 1,73 and 2.58 mW/cm^2. This work is focused on optical measurements of the SOFC anodic surface, which is why electrical properties have not been optimized for maximum efficiency. The results of electrical measurements of this cell are lower than the results of similar cells presented in the work of Kawalec [15], due to the low hydrogen content (up to 4%) in the fuel mixture in our experiment. In Fig. 3a a thermogram is presented, on which the Radius area from which the temperature in the form of distribution was recorded. Fig. 3b shows the temperature change during the loading of the cell at 1200 K determined from the ROI3 measurement field. When loading the cell from OCV to 0.0 V, it's surface temperature rises and reaches a maximum at its maximum polarization. While loading the cell in the range of 900-1200 K, the temperature change decreases and ranges from 1.05 to 0.75 K as shown on the inset of this graph. The increase of cell surface temperature during its loading was also presented by other authors [9,11]. The relatively small cell temperature increases in this work can be caused by a low-hydrogen fuel mixture. The increase in the temperature of the cell during loading is called the self-heating process and is associated with polarization losses, which are converted into heat and depend on the dynamics of heat exchange in the cell. Decreasing temperature differences (from 1.05 to 0.73 K) along with the increase of the cell operating temperature may be caused by the improvement of the effectiveness of chemical reactions, and thus by more efficient removal of heat from the system [12].

Fig. 3c presents cell load diagrams under the same conditions as above, however, data was collected from the field along the radius of the cell, marked as Radius. Differences in the temperature along the radius are visible, compared to the entire cell surface (ROI3). The highest temperature changes during loading are visible at 900 K. In the course of temperature during loading, local maxima and minima are visible, which indicate the inhomogeneity of temperature along the radius of the cell. For temperatures of 1000 to 1200 K, there is a general trend indicating that the outer surfaces of the cell have a higher temperature, due to the closer presence of the heating elements of the furnace. However, the temperature at 900 K is different, which may be the result of a chemical reaction in the cell [12].

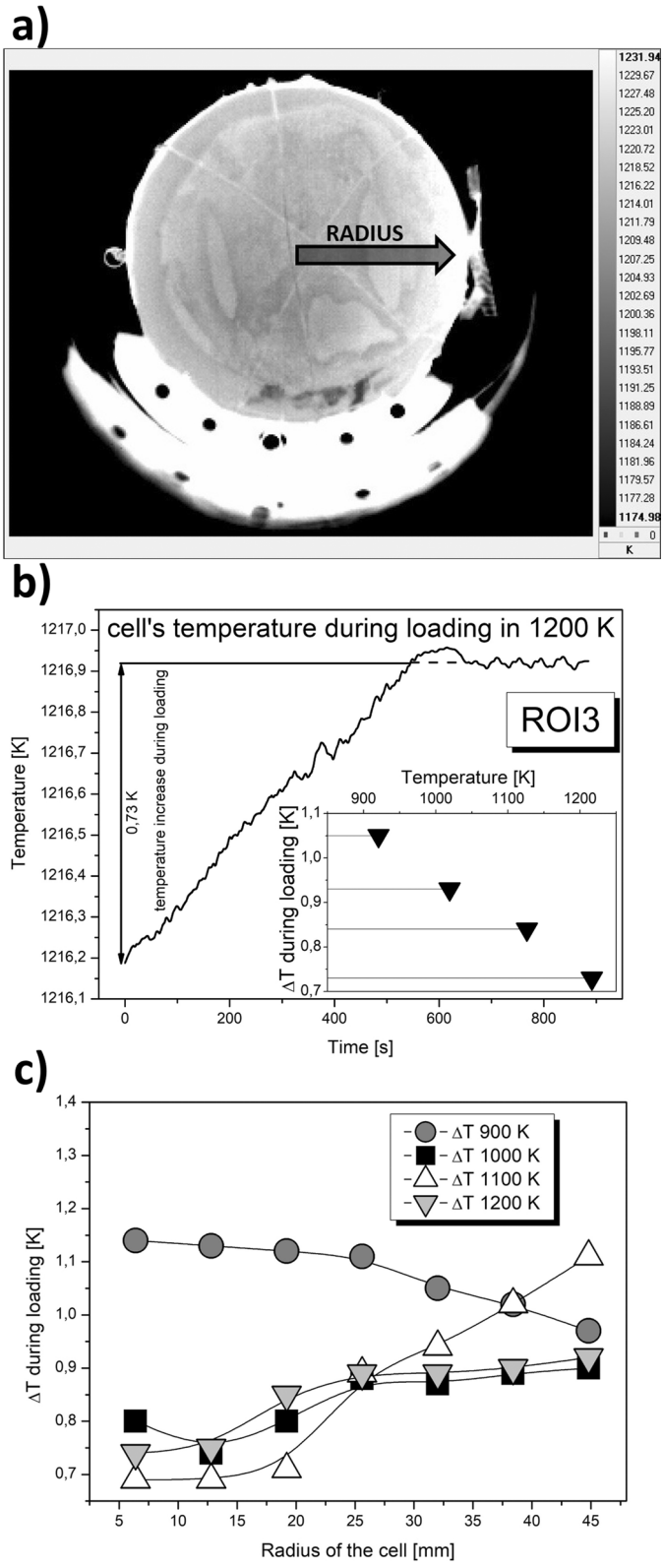

Fig. 3. Thermal image of SOFC's anode side at 1200 K – a); Radial – marked horizontal half-profile of temperature distribution. Temperature chart at 1200 K determined from the ROI3 measurement field during loading at its maximum polarization – b). Temperature change during loading of the cell at different temperatures determined from the ROI3 measurement field – inset in Fig. 3.b). Cell load diagrams collected from the field along the Radius of the cell – c)

4. Conclusions

The mid-infrared thermography method was used to study the anodic surface of a full-size SOFC type fuel cell. The results of the research are the following observations.

1. For the tested ZrO_2/Ni/NiO cells, the emissivity depends on the test temperature and decreases as the temperature rise from 0.66 at 880 K to 0.46 at 1200 K. The determined emissivity values for the cell's composite structure are higher than the emissivity of ZrO_2 and Ni in the whole studied temperature range. The emissivity level of the tested cell indicates a certain coincidence with respect to NiO, which suggests the possibility of a dynamic change in the chemical composition of the cell's surface between Ni and NiO.
2. The value of the temperature difference related to the temperature distribution in the horizontal and vertical directions increases with increasing temperature of the cell operation and for the increase of the working temperature from 800 K to 1200 K are respectively 12 K and 19 K for the horizontal direction and 14 K and 29 K for the vertical direction. This suggests that a significant influence on the temperature distribution on the surface of the working cell has a convective heat exchange. Comparison of the temperature difference values on the cell surface obtained in the current work with available data for smaller cell diameters indicates that with increasing cell diameter, there are greater differences in cell surface temperature in its profile.
3. The cell's power has been determined in the temperature range from 900 K to 1200 K from 0.51; up to 2.58 mW/cm^2. It has been determined that while loading the cell, the temperature of its surface increases and the effect of self-heating decreases with increasing temperature from 900 K to 1200 K, which may be related to the improvement of reaction efficiency occurring on the anode. It has been shown that during loading the surface temperature of the cell is inhomogeneous and may vary from 1.05 to 0.73 K, which may be due to the different efficiency of the chemical reaction in the cell.

Declaration of interest

None.

Acknowledgements

This work was supported by the National Science Centre (NCN, Poland) [grant number: UMO-2013/11/N/ST8/00834].

REFERENCES

[1] K. Alanne, A. Saari, V.I. Ugursal, J. Good, The financial viability of an SOFC cogeneration system in single-family dwellings, J. Power Sources. **158**, 403-416 (2006) doi:10.1016/j.jpowsour.2005.08.054.

[2] V. Dusastre, A. Atkinson, S. Barnett, R.J. Gorte, J.T.S. Irvine, A.J. Mcevoy, M. Mogensen, S.C. Singhal, J. Vohs, Advanced anodes for high-temperature fuel cells, Mater. Sustain. Energy. 213-223 (2012) doi:10.1142/9789814317665_0030.

[3] S. Bebelis, S. Neophytides, AC impedance study of Ni – YSZ cermet anodes in methane-fuelled internal reforming YSZ fuel cells, Solid State Ionics. **153**, 447-453 (2002).

[4] A. Bieberle, L.P. Meier, L.J. Gauckler, The Electrochemistry of Ni Pattern Anodes Used as Solid Oxide Fuel Cell Model Electrodes, J. Electrochem. Soc.) 646-656 (2001) doi:10.1149/1.1372219.

[5] D. Kim, J. Lee, T. Lim, I. Oh, H.Y. Ha, Operational characteristics of a 50 W DMFC stack, J. Power Sources. **155**, 203-212 (2006). doi:10.1016/j.jpowsour.2005.04.033.

[6] M. Adzic, M. V Heitor, D. Santos, Design of dedicated instrumentation for temperature distribution measurements in solid oxide fuel cells, J. Appl. Electrochem. **27**, 1355-1361 (1997).

[7] A. Hakenjos, H. Muenter, U. Wittstadt, C. Hebling, A PEM fuel cell for combined measurement of current and temperature distribution , and flow field flooding, J. Power Sources. **131**, 213-216 (2004). doi:10.1016/j.jpowsour.2003.11.081.

[8] M. Wang, H. Guo, C. Ma, Temperature distribution on the MEA surface of a PEMFC with serpentine channel flow bed, J. Power Sources. **157**, 181-187 (2006). doi:10.1016/j.jpowsour.2005.08.012.

[9] M.B. Pomfret, D.A. Steinhurst, D.A. Kidwell, J.C. Owrutsky, Thermal imaging of solid oxide fuel cell anode processes, J. Power Sources. **195**, 257-262 (2010). doi:10.1016/j.jpowsour.2009.06.072.

[10] M.B. Pomfret, D.A. Steinhurst, J.C. Owrutsky, Ni/YSZ solid oxide fuel cell anodes operating on humidified ethanol fuel feeds: An optical study, J. Power Sources. **233**, 331-340 (2013). doi:10.1016/j.jpowsour.2013.01.048.

[11] D.J.L. Brett, P. Aguiar, R. Clague, A.J. Marquis, S. Schöttl, R. Simpson, N.P. Brandon, Application of infrared thermal imaging to the study of pellet solid oxide fuel cells, J. Power Sources. **166**, 112-119 (2007). doi:10.1016/j.jpowsour.2006.12.098.

[12] R. Montanini, A. Quattrocchi, S.A. Piccolo, A. Amato, S. Trocino, S.C. Zignani, M. Lo Faro, G. Squadrito, Real-time thermal imaging of solid oxide fuel cell cathode activity in working condition, Appl. Opt. **55**, 7142 (2016). doi:10.1364/ao.55.007142.

[13] J.B. Robinson, L.D. Brown, R. Jervis, O.O. Taiwo, T.M.M. Heenan, J. Millichamp, T.J. Mason, T.P. Neville, R. Clague, D.S. Eastwood, C. Reinhard, P.D. Lee, D.J.L. Brett, P.R. Shearing, Investigating the effect of thermal gradients on stress in solid oxide fuel cell anodes using combined synchrotron radiation and thermal imaging, J. Power Sources. **288**, 473-481 (2015). doi:10.1016/j.jpowsour.2015.04.104.

[14] J.D. Kirtley, S.N. Qadri, D.A. Steinhurst, J.C. Owrutsky, In situ, simultaneous thermal imaging and infrared molecular emission studies of solid oxide fuel cell electrodes, J. Power Sources. **336**, 54-62 (2016). doi:10.1016/j.jpowsour.2016.10.047.

[15] M. Kawalec, R. Kluczowski, M. Krauz, Manufacturing technology of AS-SOFC prepared with different commercially avail-

able precursors, E3S Web Conf. 10 (2016) 00033. doi:10.1051/e3sconf/20161000033.

[16] P.E. Liley, Heat Exchanger Design Handbook (HEDH), Heat Exch. Des. Handb. (2019). doi:DOI 10.1615/hedhme.a.000530.

[17] Mikron Vertretung, Table of emissivity of various surfaces, (2019). www.transmetra.ch (accessed May 13, 2019).

[18] Dr Siebert & Kühn GmbH, Table of total emissivity, (2019). www.sika.net (accessed May 13, 2019).

[19] M.B. Pomfret, D.A. Steinhurst, J.C. Owrutsky, Thermal Imaging of Solid Oxide Fuel Cell Anode Degradation with Dry and Wet Ethanol Fuel Flows, ECS Trans. Electrochem. Soc. **35**, 1563-1570 (2011). doi:10.1149/1.3570141.

[20] T.L. Bergman, A.S. Lavine, F.P. Incropera, D.P. Dewitt, Fundamentals of Heat and Mass Transfer, 7th ed., John Wiley & Sons, 2011.

[21] T. Astarita, G.M. Carlomagno, Infrared Thermography for Thermo-Fluid-Dynamics, Springer-Verlag Berlin Heidelberg, 2013. doi:10.1007/978-3-642-29508-9_2.

[22] J.H. Flynn, L.A. Dunlap, Temperature gradients in horizontal tube furnaces, Thermochim. Acta. **105**, 215-218 (1986).

[23] F. Tietz, Thermal Expansion of SOFC Materials, Ionics (Kiel). **5**, 129-139 (1999).

[24] M. Mogensen, Solid Oxide Fuels Cells: Facts anf Figures, Springer, London, 2013. doi:https://doi.org/10.1007/978-1-4471-4456-4.

[25] R. Clague, P. Aguiar, D.J.L. Brett, A.J. Marquis, S. Schöttl, R. Simpson, N.P. Brandon, Application of Infrared Thermal Imaging to Map Stress Distributions in a Solid Oxide Fuel Cell, ECS Trans. Electrochem. Soc. **5**, 521-532 (2007). doi:10.1149/1.2729032.

[26] D.J. Cumming, R.H. Elder, Thermal imaging of solid oxide cells operating under electrolysis conditions, J. Power Sources. **280**, 387-392 (2015). doi:10.1016/j.jpowsour.2015.01.109.